

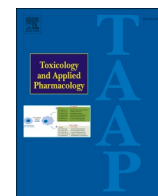
Pirfenidone attenuates acetaminophen-induced liver injury via suppressing c-Jun N-terminal kinase phosphorylation

田代, 茂樹

<https://hdl.handle.net/2324/4784478>

出版情報 : Kyushu University, 2021, 博士 (医学) , 課程博士
バージョン :
権利関係 : (c) 2021 Elsevier Inc. All rights reserved.





Pirfenidone attenuates acetaminophen-induced liver injury via suppressing c-Jun N-terminal kinase phosphorylation

Shigeki Tashiro^{a,1}, Masatake Tanaka^{a,1}, Takeshi Goya^a, Tomomi Aoyagi^a, Miho Kurokawa^a, Koji Imoto^a, Akifumi Kuwano^a, Motoi Takahashi^a, Hideo Suzuki^a, Motoyuki Kohjima^{a,*}, Masaki Kato^{a,b}, Yoshihiro Ogawa^a

^a Department of Medicine and Bioregulatory Science, Graduate School of Medical Sciences, Kyushu University, 3-1-1 Maidashi, Higashi-ku, Fukuoka 812-8582, Japan

^b Graduate School of Nutritional Sciences, Nakamura Gakuen University, 5-7-1 Befu, Jounan-ku, Fukuoka 814-0198, Japan

ARTICLE INFO

Editor: Lawrence Lash

Keywords:

Acetaminophen
Pirfenidone
JNK
Acute Liver Failure
Cell Death

ABSTRACT

Acetaminophen (APAP)-induced liver injury is the most frequent cause of acute liver failure in Western countries. Pirfenidone (PFD), an orally bioavailable pyridone derivative, is clinically used for idiopathic pulmonary fibrosis treatment and has antifibrotic, anti-inflammatory, and antioxidant effects. Here we examined the PFD effect on APAP-induced liver injury.

In a murine model, APAP caused serum alanine aminotransferase elevation attenuated by PFD treatment. We performed terminal deoxynucleotidyl transferase-mediated deoxyuridine triphosphate nick-end labeling (TUNEL) and vital propidium iodide (PI) stainings simultaneously. APAP induced TUNEL-positive/PI-negative necrosis around the central vein and subsequent TUNEL-negative/PI-positive oncotic necrosis with hemorrhage and caused the upregulation of hypercoagulation- and hypoxia-associated gene expressions. PFD treatment suppressed these findings. Western blotting revealed PFD suppressed APAP-induced c-Jun N-terminal kinase (JNK) phosphorylation despite no effect on JNK phosphatase expressions.

In conclusion, simultaneous TUNEL and vital PI staining is useful for discriminating APAP-induced necrosis from typical oncotic necrosis. Our results indicated that PFD attenuated APAP-induced liver injury by suppressing TUNEL-positive necrosis by directly blocking JNK phosphorylation. PFD is promising as a new option to prevent APAP-induced liver injury.

1. Introduction

Acetaminophen (*N*-acetyl-*p*-aminophenol, APAP) is an extensively used analgesic and antipyretic drug in the world. APAP is considered safe at therapeutic dose because it has a lower rate of adverse effects than that of nonsteroidal anti-inflammatory drugs (NSAIDs). However,

APAP overdose frequently causes acute liver injury (Thomas, 1993) which may progress to acute liver failure (ALF) (Larson, 2007). In fact, APAP-induced liver injury is responsible for almost 50% of ALF cases in the United States and Western Europe (Bernal et al., 2010; Lee, 2012, 2017). *N*-acetyl-L-cysteine (NAC) is the only drug which can prevent APAP hepatotoxicity. Its administration needs to be within 8 h after

Abbreviations: ActD, Actinomycin D; ALF, acute liver failure; ALT, alanine aminotransferase; APAP, *N*-acetyl-*p*-aminophenol; ASK1, apoptosis signal-regulating kinase 1; GalN, D-galactosamine; GAPDH, glyceraldehyde 3-phosphate dehydrogenase; GSH, glutathione; GSSG, glutathione disulfide; H&E staining, hematoxylin and eosin staining; HBSS, Hank's balanced salt solution; HIF1 α , hypoxia inducible factor 1 α ; HRP, horse radish peroxidase; HO-1, heme oxygenase-1; JNK, c-Jun N-terminal kinase; LPS, Lipopolysaccharide; MAPK, mitogen-activated protein kinase; MKK4, mitogen-activated protein kinase kinase 4; MKP-1, mitogen-activated protein kinase phosphatase-1; MLK3, mixed-lineage kinase 3; NAC, *N*-acetyl-L-cysteine; NAPQI, *N*-acetyl-*p*-benzoquinone imine; Nrf-2, Nuclear factor erythroid 2-related factor 2; NSAIDs, nonsteroidal anti-inflammatory drugs; PAI-1, plasminogen activator inhibitor-1; PBS, phosphate-buffered saline; PCR, polymerase chain reaction; PFD, pirfenidone; PI, propidium iodide; pJNK, phosphorylated JNK; pMKK4, phosphorylated MKK4; PVDF, polyvinylidene fluoride; ROS, reactive oxygen species; SEC, sinusoidal endothelial cell; SD, standard deviation; SDS-PAGE, sodium dodecyl sulfate-polyacrylamide gel electrophoresis; SEM, standard error of the means; TF, tissue factor; TNF α , Tumor Necrosis Factor α ; TUNEL, terminal deoxynucleotidyl transferase-mediated deoxyuridine triphosphate nick-end labeling.

* Corresponding author.

E-mail address: kohjima@med.kyushu-u.ac.jp (M. Kohjima).

¹ contributed equally to this work.

<https://doi.org/10.1016/j.taap.2021.115817>

Received 19 August 2021; Received in revised form 29 November 2021; Accepted 2 December 2021

Available online 8 December 2021

0041-008X/© 2021 Elsevier Inc. All rights reserved.

APAP ingestion (Fisher and Curry, 2019). Therefore, the development of new treatments is urgently necessitated.

Recently, Jaeschke et al. intensively reviewed the modes of APAP-induced cell death (Jaeschke et al., 2019), which presents the histological features of oncotic necrosis, such as cell swelling, plasma membrane integrity loss, and extracellular leakage of cellular components. However, it is accompanied by DNA fragmentation, distinguishing APAP-induced cell death from the typical oncotic necrosis. Terminal deoxynucleotidyl transferase-mediated deoxyuridine triphosphate nick-end labeling (TUNEL) staining, a widely used method to detect fragmented DNA, is well known to be positive for the nucleus of apoptotic cells, while TUNEL is positive for the cytoplasm and nucleus in APAP-induced cell death (Gujral et al., 2002). Collectively, the authors proposed APAP-induced cell death should be termed “programmed necrosis.”

In 2016, Imagawa et al. reported the vital propidium iodide (PI) staining method, in which PI solution is injected into mice in vivo. Necrotic cells were detected as PI-positive cells in tissue sections (Imagawa et al., 2016). Several reports showed that necrotic cells were identified using PI solution in APAP induced liver injury. (Wimborne et al., 2020; Hu and Lemasters, 2020). In this study, we simultaneously performed vital PI and TUNEL stainings on mice with APAP-induced liver injury.

Pirfenidone (PFD) is an orally bioavailable pyridone derivative and is approved for idiopathic pulmonary fibrosis treatment (Rosenbloom et al., 2013). However, the molecular mechanism has not been elucidated yet. Here we examined PFD's effect on APAP-induced liver injury by in vivo and in vitro experiments.

2. Material and methods

2.1. Animals

Eight-week-old male C57B/6 J mice were obtained (Japan SLC, Inc. (Shizuoka, Japan)) and maintained under controlled conditions with access to water and food in an ordinary cage at a normal room temperature (25 °C) and relative humidity of about 50% with a 12-h light/dark cycle. The mice were fasted overnight and randomly divided into two groups ($n = 5$ per group) the night before the experiments. (1) In the APAP group, the mice were administrated with APAP (300 mg/kg) intraperitoneally and saline intragastrically. (2) In the APAP + PFD group, the mice were administrated APAP (300 mg/kg) intraperitoneally and PFD (30 mg/kg) intragastrically. Liver injury was reported one of the adverse effects of PFD. To minimize the hepatotoxic effect, 30 mg/kg PFD was administrated to the mouse based on the lower end of the dose-response curve of the approval submitted to the FDA. All animals were euthanized with isoflurane. Blood and liver tissue samples were collected at 3, 6, 12, and 24 h after APAP administration. PFD was provided by Shionogi & Co., Ltd. (Osaka, Japan). All studies were performed following the *Guide for the Care and Use of Laboratory Animals* (National Institutes of Health) with approval from Kyushu University's Animal Care Committee.

2.2. Blood sample and biochemical analysis

Serum alanine aminotransferase (ALT) levels were measured using DRI-CHEM NS500sV (FUJIFILM, Tokyo, Japan). Glutathione (GSH) and glutathione disulfide (GSSG) were measured in liver homogenate using GSSG/GSH Quantification Kit (Dojindo, Kumamoto, Japan) according to the manufacturer's protocol.

2.3. Histological analysis

Formalin-fixed liver tissues were embedded in paraffin and cut into 5- μ m sections. General histology was examined using hematoxylin and eosin (H&E) staining. TUNEL staining was performed using Apoptosis

Detection Kit (Takara Bio Inc., Shiga, Japan) following the manufacture's protocol to detect DNA-fragmented cells. The vital PI staining method was employed (Imagawa et al., 2016; Tsurusaki et al., 2019) to detect liver necrotic cells. Briefly, 25 μ g/mL PI solution dissolved in phosphate-buffered saline (PBS) was intravenously injected into mice via the tail vein 2 h before sacrificing. Liver samples were fixed in 4% formalin, embedded in paraffin, sectioned, and analyzed using a fluorescence microscope (BZ-X710, KEYENCE, Japan).

2.4. Reverse transcription-quantitative PCR

The liver tissue total RNA was isolated using TRIzol reagent (Invitrogen, Carlsbad, CA). cDNA was synthesized using GeneAmp RNA polymerase chain reaction (PCR) (Applied Biosystems, Branchburg, NJ). Real-time PCR was performed using LightCycler FastStart DNA Master SYBR Green I (Roche, Basel, Switzerland). All data were normalized to glyceraldehyde 3-phosphate dehydrogenase (GAPDH) expression, controlling reaction variations. Relative expression was presented using the $2^{-\Delta\Delta C_t}$ method. The primer sequences are listed in Table 1.

2.5. Western blotting

The liver tissues were homogenized in the lysis buffer (20 mM pH 7.6 Tris HCl, 150 mM NaCl, 0.5% NP-40, 2 mM EDTA containing protease and phosphatase inhibitor cocktails). To separately evaluate protein expressions in the mitochondria and cytosol, the Mitochondria Isolation Kit for Tissue (ab110168, abcam, Cambridge, England), according to the manufacturer's protocol, separated the mitochondrial and cytosolic fractions. The homogenized tissues were sonicated for 1 min and then centrifuged at 12,000 $\times g$ for 20 min at 4 °C. Sodium dodecyl sulfate-polyacrylamide gel electrophoresis (SDS-PAGE) was used to separate the protein, followed by electroblotting onto the polyvinylidene fluoride (PVDF) membrane. After blocking in 5% fat-free milk solution for 1 h and rinsing thrice with Tris buffer (0.05 M Tris HCl, 0.138 M NaCl, 2.7 mM KCl, and 1% Tween-20), the membrane was probed with primary antibodies overnight at 4 °C and incubated with the horseradish peroxidase (HRP)-conjugated secondary antibody for 1 h at room temperature. All primary and secondary antibodies were purchased from the Cell Signaling Technology (Boston, MA): rabbit anti-c-Jun N-terminal kinase (JNK) (1:1000 dilution, #9252S), anti-phospho-JNK (1:1000, #9251S), anti-mitogen-activated protein kinase kinase 4 (MKK4) (1:1000, #9152S), anti-phospho-MKK4 (1:1000, #4514S), anti-mitogen-activated protein kinase phosphatase-1 (MKP-1) (1:1000, #35217S), anti- β actin (1:1000, #4970S) monoclonal antibodies and goat anti-rabbit IgG HRP-conjugated polyclonal antibody (1:1000, #7074S). Immune complexes were visualized using the enhanced chemiluminescence system. Protein band intensity was analyzed using the ImageJ software (National Institutes of Health, Bethesda, MD).

2.6. Reactive oxygen species (ROS) quantification in liver tissue

The concentration of ROS in liver tissue was quantified using the method described by Niknahad et al. (Niknahad et al., 2017), with some modifications. Briefly, 200 mg of liver tissue were homogenized in 2 mL

Table 1
Primers for real-time PCR.

Genes	Forward (5'–3')	Reverse (5'–3')
GAPDH	TGTGTCCGTCGTGGATCTGA	TTGCTGTTGAAGTCGACGAG
PAI-1	TCTGGGAAAGGGTTCACTTTACC	GACACGCCATAGGGAGAGAAG
TF	TGCTTCTCGACCACAGACAC	TAAAAACTTTGGGGCGTTTG
HO-1	ACGCATATACCCGCTACCTG	AAGGCGGTCTTAGCCTCTTC
HIF1 α	AGCTTCTGTTATGAGGCTCACC	TGACTTGATGTTTCATCGTCCTC

GAPDH, glyceraldehyde 3-phosphate dehydrogenase; PAI-1, plasminogen activator inhibitor-1; TF, tissue factor; HO-1, heme oxygenase-1; HIF1 α , hypoxia inducible factor 1 α .

of ice-cold Tris-HCl buffer (40 mM, pH = 7.4). Tissue homogenates (100 μ L) were incubated for 40 min at 37 °C with 1 mL of a solution of 2,7-dichlorofluorescein diacetate (final concentration: 10 μ M) diluted 1:200 in Tris-HCl buffer. As control of tissue autofluorescence, 100 μ L of tissue homogenate were incubated with 1 mL of Tris-HCl buffer in the same conditions. The fluorescence intensity was measured at an excitation and emission wavelength of 485 nm and 525 nm, respectively, using an Enspire multimode plate reader (PerkinElmer, Waltham, USA).

2.7. Isolation and culture of primary hepatocyte

Primary hepatocytes were isolated and cultured as previously described (Maeda et al., 2003). Following the exposed portal vein cannulation, the mouse liver was pre-perfused in situ with Hank's balanced salt solution (HBSS) containing 0.5 mM EGTA and 0.01 M HEPES to remove the blood. The liver was perfused with collagenase solution (0.08% collagenase in DMEM). After liver extraction, the cells were dispersed in DMEM by blade mincing. Obtained cells were filtered through a 70- μ m pore mesh nylon cell strainer (FALCON, Corning, NY) and centrifuged twice for 2 min at 100 \times g to remove nonparenchymal cells. Subsequently, cell viability was measured using the trypan blue method. The isolated hepatocytes were suspended and plated at the appropriate cell density with DMEM containing 10% (v/v) heat-inactivated fetal bovine serum, 100 U/mL penicillin, 100 g/mL streptomycin, 1.2 mg/L insulin, and 0.25 mM L-ascorbic acid 2-phosphate sesquimagnesium salt hydrate. The cells were incubated at 37 °C in a humidified incubator with 5% CO₂/95% air. The cell attachment medium was replaced with a fresh medium after the first 4-h incubation. On the next day, the growth medium was exchanged with a serum-free medium, which was replaced daily thereafter. APAP and PFD were dissolved in warm PBS and added to the medium. For the experiment, the primary culture hepatocytes were incubated with 5 mM APAP and 1 mM PFD. The concentration of PFD was determined by referring to previous report (Komiya et al., 2017). The author demonstrated PFD exhibited a dose-dependent inhibitory effect on cell death. We used 1 mM, which is the maximum concentration of PFD in the report. PFD was administered 3 h before APAP administration. The samples were collected at 0, 1, 2, and 3 h after APAP administration.

2.8. Statistical analysis

Data were analyzed using the JMP Pro Version 15 statistical software (SAS Institute Inc., Cary, NC), with results expressed as means and standard deviation (SD) or standard error of the means (SEM). Significant differences between the groups were assessed using the unpaired Student's *t*-test. Mean differences among multiple groups were analyzed using the one-way ANOVA and Tukey's post hoc test. *P* < 0.05 indicated statistical significance.

3. Result

3.1. PFD suppressed ALT elevation in mice with APAP-induced liver injury

First, we measured the serum ALT concentration to evaluate the effect of PFD on APAP-induced liver injury. In the APAP group, the serum ALT level was elevated 3 h after APAP treatment and continuously increases in a time-dependent manner (Fig. 1). The ALT level in the APAP + PFD group was significantly lower than that of the APAP group at 12 and 24 h after APAP administration.

3.2. PFD suppressed APAP-induced TUNEL-positive necrosis around the central vein and subsequent hemorrhagic necrosis

Next, we performed H&E staining for general histology, TUNEL staining for DNA-fragmented cell detection, and vital PI staining for

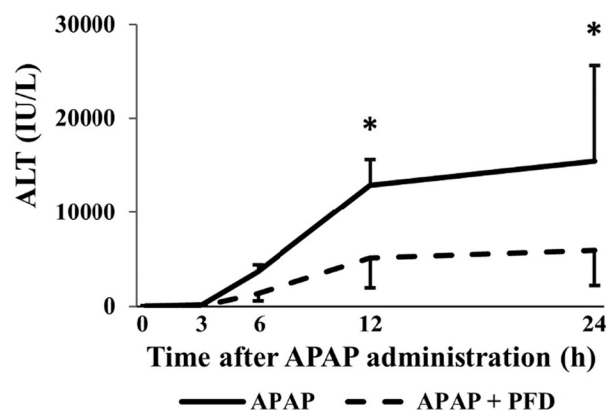


Fig. 1. PFD attenuated serum ALT elevation after APAP administration.

After an 18-h fast, APAP and saline or PFD (300 and 30 mg/kg) were simultaneously administered to mice intraperitoneally and orally, respectively. Mice were sacrificed at 3, 6, 12, and 24 h after APAP administration. Serum ALT levels were then measured. Results are expressed as mean \pm SD of *n* = 5 animals per group; * *P* < 0.05.

necrotic cell detection. In the APAP group, necrotic features, including pale eosinophilic staining and nuclei loss, appeared in hepatocytes around the central vein (zone 3) 3 h after APAP administration, which developed in a time-dependent manner (Fig. 2A). Eventually, hemorrhagic oncotoc necrosis (hemorrhagic necrosis) and sinusoidal congestion were observed throughout the liver lobes 24 h after APAP administration. APAP-induced necrotic cells, whose cytoplasm was positive for TUNEL staining, gradually increased in zone 3 after 6–12 h and disappeared after 24 h. Vital PI staining revealed a negative PI for cells under APAP-induced necrosis, while those under hemorrhagic necrosis 24 h after APAP administration were positive. These findings indicated the simultaneously evaluating TUNEL and vital PI staining is a novel histological method in distinguishing APAP-induced and typical oncotoc necroses.

PFD administration drastically decreased the APAP-induced necrotic area in the early phase H&E and TUNEL staining (Fig. 2B). Moreover, PFD completely suppressed PI-positive hemorrhagic necrosis 24 h after APAP administration (Fig. 2B).

3.3. PFD attenuated gene expression associated with hypercoagulation and hypoxia

Next, we evaluated the gene expression levels associated with hypercoagulation and hypoxia using the reverse transcription-quantitative PCR method. The PAI-1 gene expression level associated with hypercoagulation significantly increased 12 h after APAP administration, which developed in a time-dependent manner (Fig. 3A). The gene expression level of TF, initiating the coagulation cascades, present no significant difference between time points (Fig. 3B). The expression level of hypoxic genes, HO-1 and HIF1 α , significantly increased 12 h and decreased 24 h after APAP administration (Fig. 3C–D). PFD treatment significantly suppressed the gene expressions of PAI-1 (Fig. 3A) and HIF1 α and HO-1 24 and 12 h after APAP administration, respectively (Fig. 3C–D).

3.4. PFD did not affect GSH metabolism by APAP

APAP hepatotoxicity is induced by the formation of *N*-acetyl-p-benzoquinone imine (NAPQI), a CYP2E1-generated APAP metabolite (McGill and Jaeschke, 2013). NAPQI is rapidly scavenged by GSH in a normal condition. However, massive NAPQI due to APAP overdose depletes cellular GSH.

We found that the hepatic GSH level drastically decreased as early as

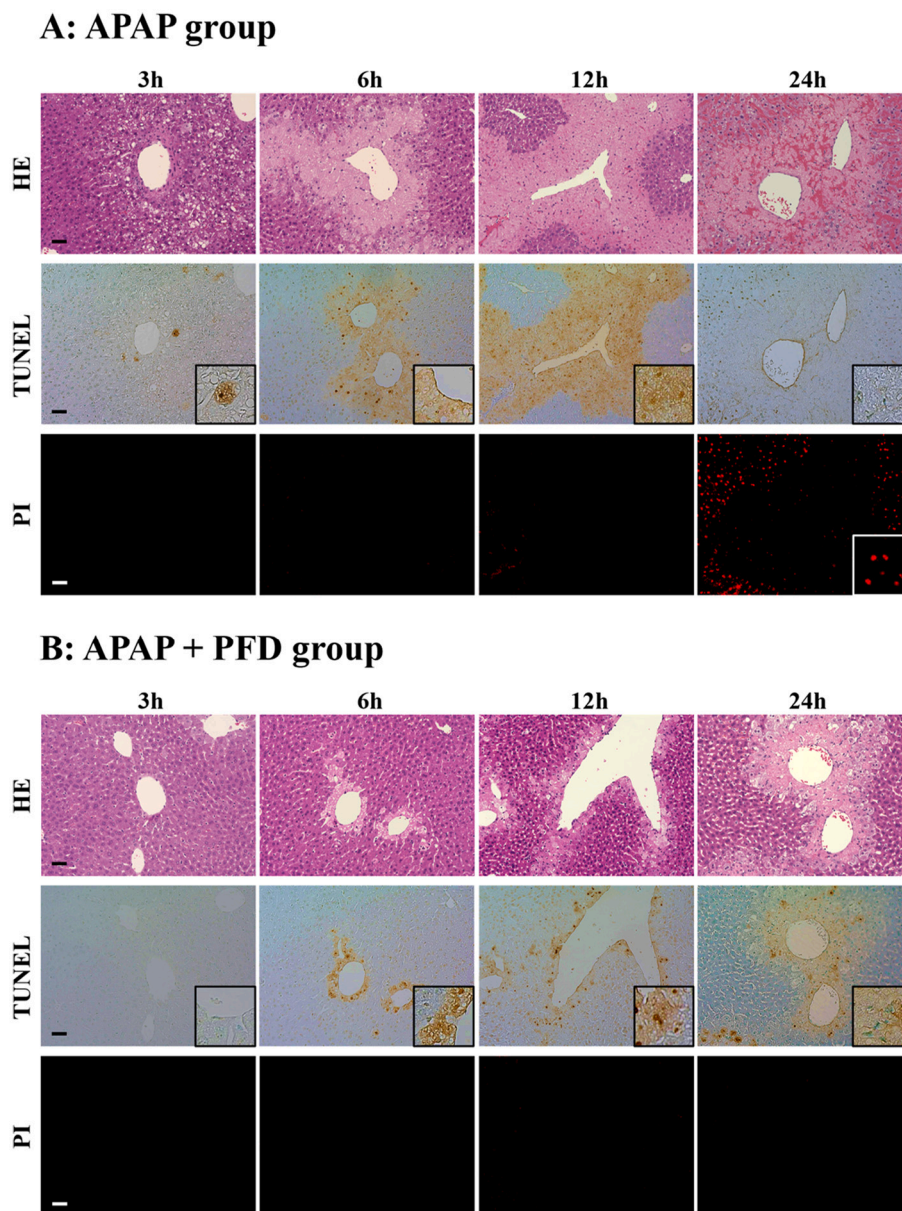


Fig. 2. Microscopic images of hematoxylin and eosin (H&E), TUNEL, and vital PI staining of the liver sections.

In the APAP group (A), TUNEL-positive/PI-negative hepatocyte necrosis around the central vein appeared 3 h after APAP administration, which developed in a time-dependent manner. After 24 h, TUNEL-negative/PI-positive hemorrhagic necrosis with congestion was observed throughout the liver lobes. In the APAP + PFD group (B), TUNEL-positive/PI-negative hepatocyte necrosis was attenuated, and TUNEL-negative/PI-positive hemorrhagic necrosis was completely suppressed. Representative hepatic sections of $n = 3$ –5 animals per group—scale bar: 50 μ m.

1.5 h after APAP administration (Fig. 4). The hepatic GSH levels between the APAP and APAP + PFD groups displayed no significant difference, suggesting that PFD does not affect APAP metabolism by CYP2E1 (Fig. 4).

3.5. PFD suppressed APAP-induced liver injury by inhibiting activation of JNK

NAPQI, which overwhelmed the GSH scavenging capacity, generates ROS and phosphorylates JNK in the cytosol. Phosphorylated JNK (pJNK) migrates to the mitochondria, causing mitochondrial dysfunction and aggregated oxidative stress (Hanawa et al., 2008).

We evaluated pJNK and JNK protein levels using Western blotting. The pJNK/JNK ratio, reflecting JNK activation, increased 3 h after APAP administration, while PFD treatment significantly suppressed the pJNK/JNK ratio increase (Fig. 5A). The chronological evaluation of the pJNK/JNK ratio revealed that PFD's suppressive effect on JNK phosphorylation was only observed in the early phase 3 h after APAP administration (Fig. 5B). PFD significantly suppressed the pJNK/JNK ratio increase in both cytosolic and mitochondrial fractions 3 h after APAP

administration (Fig. 5C), suggesting that PFD treatment also suppressed pJNK translocation to the mitochondria. At 3 h after APAP administration when PFD inhibited JNK phosphorylation, APAP administration generated ROS significantly compared to control. While PFD treatment had no effect on ROS production in liver tissue with APAP administration (Fig. 5D).

3.6. PFD did not affect the expressions of MKK4 phosphatases in liver tissue, while translocation of pMKK4 to mitochondria was attenuated by PFD treatment

Next, we evaluated the expression of JNK phosphatases to elucidate PFD's action site. Mitogen-activated protein kinase kinase 4 (MKK4) is a stress-activated MAP kinase signaling module component and directly phosphorylates JNK (Zhang et al., 2017). On the other hand, mitogen-activated protein kinase phosphatase-1 (MKP-1) preferentially dephosphorylates pJNK, reported to have an APAP-induced liver injury protective effect (Hammer et al., 2006; Wancket et al., 2012).

We found MKK4 was significantly phosphorylated 3 h after APAP administration. PFD did not suppress MKK4 phosphorylation (Fig. 6A).

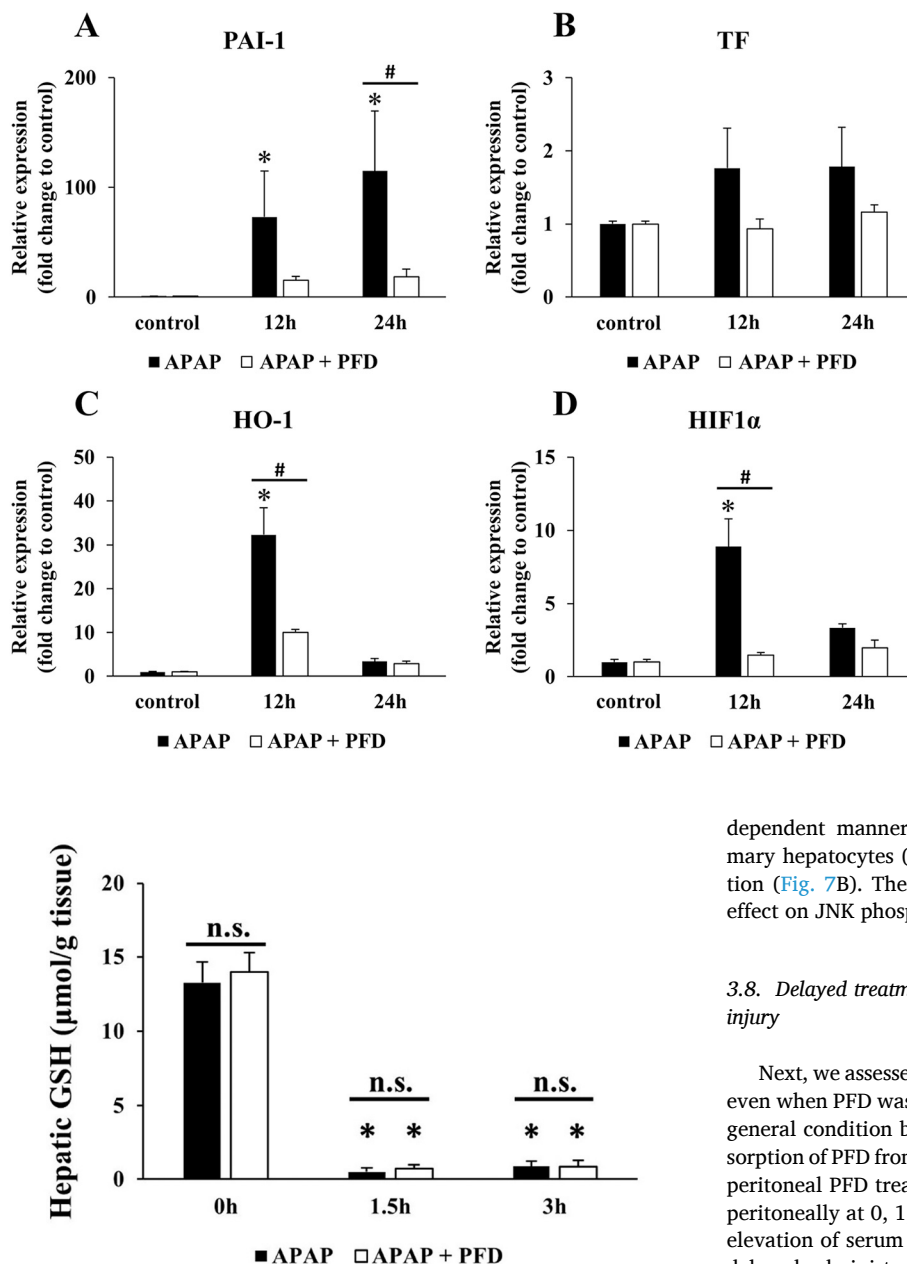


Fig. 4. PFD did not affect the hepatic GSH level, which drastically decreased after APAP administration. GSH contents were measured using mouse liver samples of 0, 1.5, and 3 h after APAP administration. The results are expressed as mean \pm SD of $n = 3-5$ animals per group: * $P < 0.05$ compared to control.

The pMKK4/MKK4 ratio's chronological study also demonstrated no significant difference between the APAP and APAP + PFD groups until 24 h after APAP administration (Fig. 6B). On the other hand, PFD inhibited translocation of pMKK4 to mitochondria 3 h after APAP administration (Fig. 6C). MKP-1 expression was not affected by either APAP administration or PFD treatment (Fig. 6D).

3.7. PFD inhibited the phosphorylation of JNK in culture primary hepatocytes

To confirm that PFD suppression of JNK phosphorylation occurs in hepatocytes, not in nonparenchymal cells, we performed an in vitro experiment using primary hepatocytes. Identical to in vivo experiment results, JNK was phosphorylated after APAP administration in a time-

dependent manner, and PFD inhibited JNK phosphorylation in primary hepatocytes (Fig. 7A). PFD did not suppress MKK4 phosphorylation (Fig. 7B). These results indicated that PFD exerts its suppressive effect on JNK phosphorylation in hepatocytes.

3.8. Delayed treatment with PFD also suppressed APAP-induced liver injury

Next, we assessed whether PFD suppresses APAP induced liver injury even when PFD was administered later. Because the exacerbation of the general condition by APAP induced liver injury could suppress the absorption of PFD from the gastrointestinal tract, we evaluated the effect of peritoneal PFD treatment. PFD was dissolved in PBS and administered peritoneally at 0, 1, 2, and 4 h after APAP injection. We found that the elevation of serum ALT was significantly suppressed in All groups and delayed administration of PFD attenuated APAP induced liver injury (Fig. 8). The group that received PFD 4 h after APAP administration showed significantly severe liver damage compared with the group received PFD simultaneously. These findings suggested that delayed administration of PFD was also effective in APAP hepatotoxicity, and early treatment of PFD had more intensive suppressive effect on APAP-induced liver injury.

4. Discussion

Various types of cell death have been reported to be involved in APAP-induced liver injury, such as apoptosis (Ferret et al., 2001; Kanno et al., 2000; Ray et al., 1996; Zhang et al., 2000), necrosis (Gujral et al., 2002), necroptosis (Dara et al., 2015; Ramachandran et al., 2013; Zhang et al., 2014), and ferroptosis (Yamada et al., 2020). As mentioned earlier, Jaeschke et al. intensively reviewed the APAP-induced cell death modes (Jaeschke et al., 2019) and were convinced that APAP-induced cell death is programmed necrosis with cytoplasmic TUNEL positivity. In 2016, Imagawa et al. established the vital (PI) staining method to detect necrotic cells (Imagawa et al., 2016). PI solution was intravenously injected into mouse embryos, and frozen tissue sections were

Fig. 3. PFD attenuated APAP-induced hypercoagulation- and hypoxia-associated gene expression upregulation.

The mRNA expression levels of PAI-1 (A), TF (B), HO-1 (C), and HIF1α (D) were evaluated using quantitative reverse transcription PCR and were normalized to GAPDH as a reference gene. The data was presented by fold changes to 0 h as mean \pm SEM of $n = 3-5$ animals per group: * $P < 0.05$ compared to control and # $P < 0.05$ APAP group vs. APAP + PFD group.

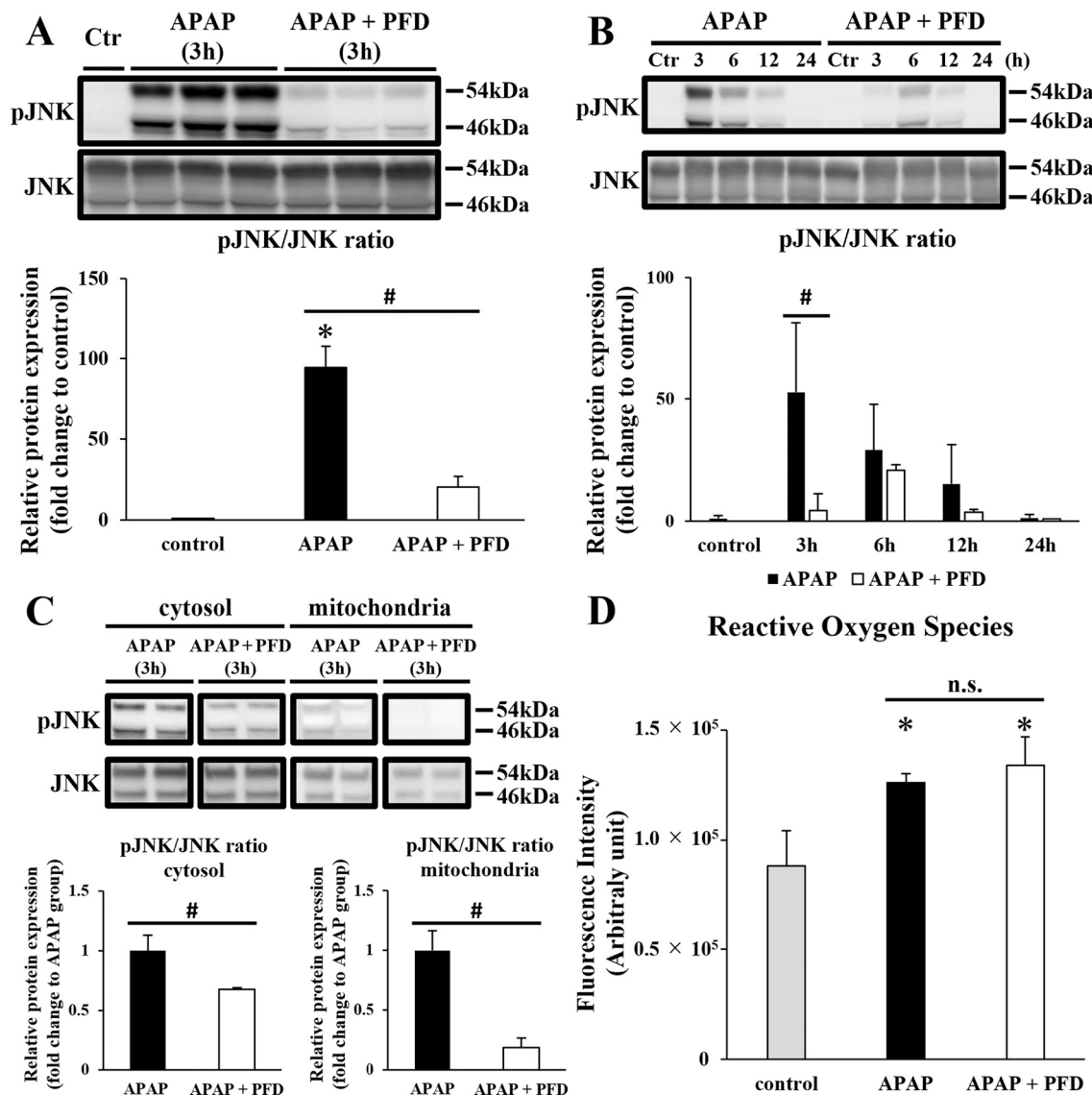


Fig. 5. PFD suppressed JNK phosphorylation induced by APAP administration in the mouse liver.

JNK and pJNK Western blotting was performed, and the pJNK/JNK ratio in the mouse liver was calculated. PFD suppressed JNK phosphorylation 3 h after APAP administration (A). The chronological evaluation revealed that PFD's suppressive effect was only observed 3 h after APAP administration. The data represented the average from three independent experiments (B). PFD significantly suppressed the pJNK/JNK ratio increase in both cytosolic and mitochondrial fractions 3 h after APAP administration. The data represented the average from three independent experiments (C). PFD did not affect ROS production 3 h after APAP administration. $n = 3$ animals per group (D). The results are expressed as mean \pm SD. * $P < 0.05$ compared to control and # $P < 0.05$ APAP group vs. APAP + PFD group.

prepared. Since PI has membrane permeability to necrotic cells, not to vital cells, fluorescent microscopy could identify necrotic cells as PI-positive cells. Several reports showed that necrotic cells were identified using PI solution in APAP induced liver injury (Wimborne et al., 2020; Hu and Lemasters, 2020). We performed vital PI staining simultaneous with TUNEL staining on mice with APAP-induced liver injury to distinguish the type of cell death. TUNEL-positive cell death around zone 3 appeared from the early phase after APAP administration; the hemorrhagic necrosis with congested and dilated sinusoids was observed throughout the liver lobes 24 h after APAP administration (Fig. 2A). In vital PI staining, revealed that the cells under APAP-induced TUNEL-positive necrosis and those under hemorrhagic necrosis 24 h after APAP administration were negative and positive, respectively, for PI. We demonstrated the usefulness of the simultaneous TUNEL and vital PI staining in discriminating APAP-induced necrosis from typical oncotic necrosis. Mitochondrial dysfunction may trigger both necrosis and apoptosis. Although necrosis is responsible for most of the cell death

in APAP liver injury, the possibility of apoptotic involvement is controversial. One of essential factor for the progression of apoptotic signaling is the mitochondrial release of cytochrome *c* to cytosol. Here, APAP administration caused the release of cytochrome *c* from mitochondria to cytosol and PFD had no effect on the cytochrome *c* release (Fig. S1). Meanwhile caspases are directly or indirectly responsible for all aspects of apoptotic signaling and procaspase processing and caspase enzyme activities are the most specific indicators of apoptotic cell death (Julien and Wells, 2017; Thornberry, 1997). Previous studies assessing caspase activation could not find any evidence for increased caspase-3 activity, the main executioner caspase, during APAP hepatotoxicity in vivo (Adams et al., 2001; Lawson et al., 1999), and more importantly, pan-caspase inhibitors had no effect on APAP-induced liver injury (Gujral et al., 2002; Lawson et al., 1999; Jaeschke et al., 2006). Similar findings were also found in primary human hepatocytes (Xie et al., 2014), human HepaRG cells (McGill and Jaeschke, 2013) and patients (Antoine et al., 2012; McGill et al., 2012). These findings suggest that

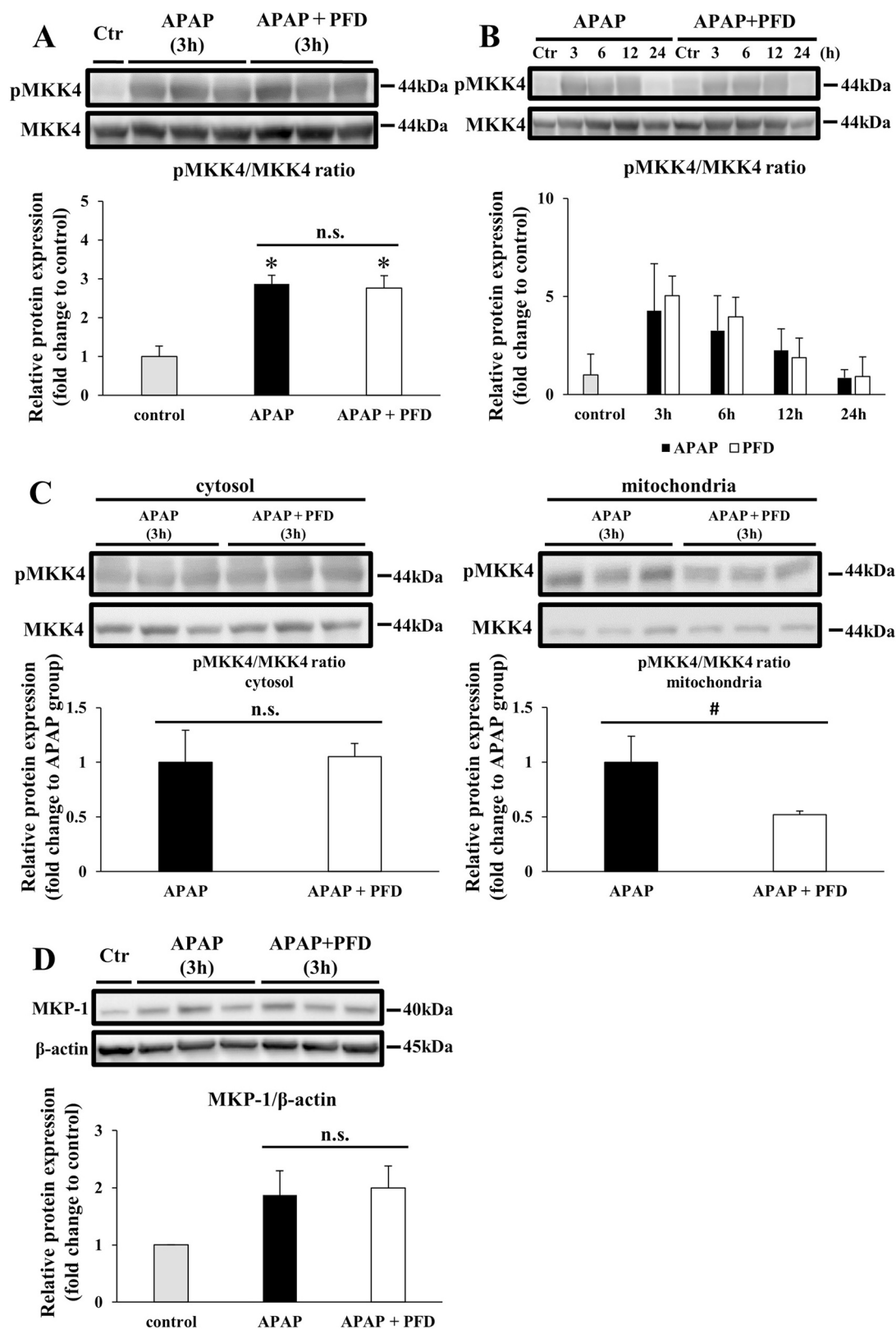


Fig. 6. PFD did not affect the MKK4 phosphorylation and MKP-1 expression in the mouse liver.

MKK4 and phosphorylated MKK4 (pMKK4) Western blotting was performed and pMKK4/MKK4 ratio calculated. APAP administration significantly increased pMKK4/MKK4 ratio 3 h after APAP administration; PFD did not affect MKK4 phosphorylation (A). The chronological evaluation also demonstrated that PFD did not affect MKK4 phosphorylation. The data represented the average from three independent experiments (B). Phosphorylation of MKK4 in mitochondria was attenuated by PFD treatment 3 h after APAP administration (C). MKP-1 Western blotting showed that either APAP administration or PFD treatment did not affect MKP-1 expression 3 h after APAP administration (D). The results are expressed as mean \pm SD. * P < 0.05 compared to control and # P < 0.05 APAP group vs. APAP + PFD group.

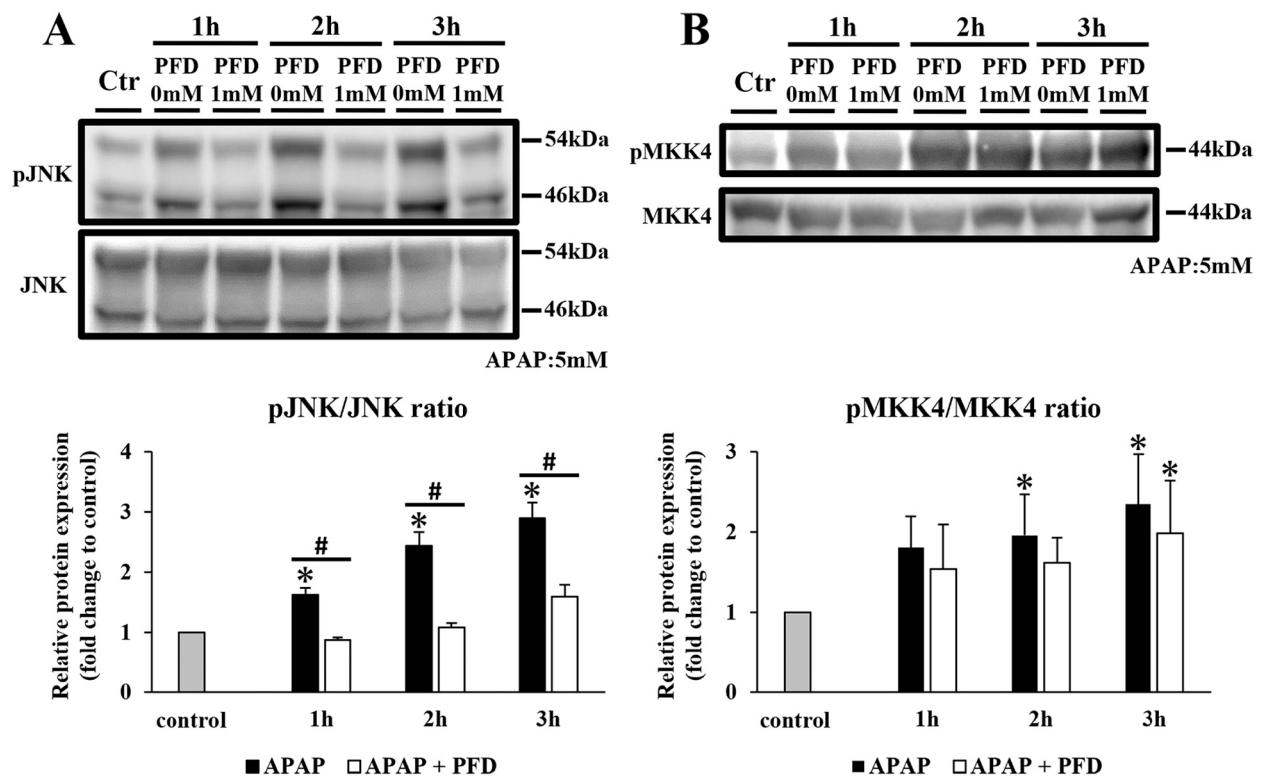


Fig. 7. PFD suppressed JNK phosphorylation and did not affect MKK4 phosphorylation in APAP-treated primary hepatocytes.

Primary hepatocytes were treated with 5 mM APAP with or without 1 mM PFD and harvested 1, 2, and 3 h later. JNK and pJNK Western blotting demonstrated that JNK was phosphorylated after APAP treatment in a time-dependent manner, and PFD inhibited JNK phosphorylation (A). MKK4 and pMKK4 Western blotting demonstrated that PFD did not affect MKK4 phosphorylation (B). The data represented the average from three independent experiments. The results are expressed as mean \pm SD. * $P < 0.05$ compared to control and # $P < 0.05$ APAP group vs. APAP + PFD group.

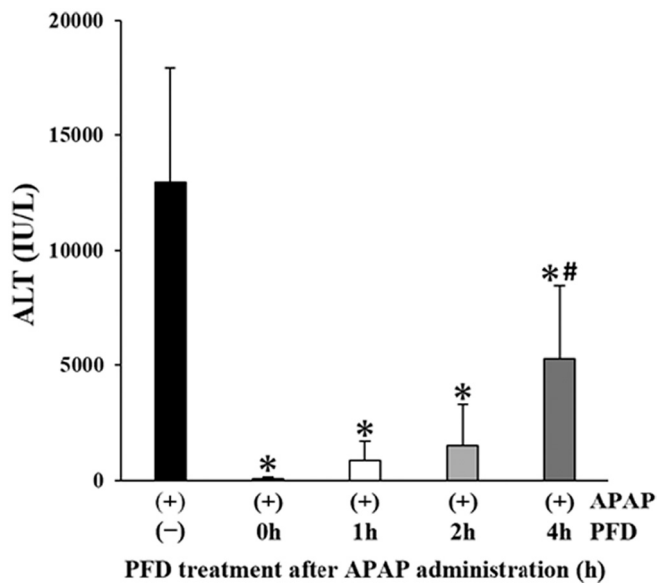


Fig. 8. Delayed treatment with PFD suppressed APAP-induced liver injury.

After an 18-h fast, PFD (30 mg/kg) was administered intraperitoneally at 0, 1, 2, and 4 h after APAP (300 mg/kg) administration. Mice were sacrificed at 12 h after APAP administration. Serum ALT levels were measured. Results are expressed as mean \pm SD of $n = 4-6$ animals per group. * $P < 0.05$ compared to APAP group and # $P < 0.05$ compared to group that simultaneously administered APAP and PFD.

there is no relevant apoptotic cell death contributing to APAP-induced liver injury (Jaeschke et al., 2018) and the release of cytochrome *c* into cytosol observed in this study might not cause apoptotic cell death.

APAP therapeutic dose is metabolized mainly by glucuronidation and sulfation in hepatocytes. Only a minor part of APAP is converted by cytochrome P450 enzymes to NAPQI, which is immediately scavenged by GSH (Fig. 9). NAPQI is highly toxic due to its aggressive reactivity with proteins (McGill and Jaeschke, 2013). APAP overdose overwhelmed glucuronidation and sulfation capacities. A large amount of APAP is converted into NAPQI. Massive NAPQI depletes cellular GSH; covalently binds to proteins, especially mitochondria; and triggers mitochondrial oxidative stress (McGill et al., 2013). Oxidative stress activates MAP kinase kinase, such as apoptosis signal-regulating kinase 1 (ASK1) and mixed-lineage kinase 3 (MLK3), and subsequently, MAP kinase kinase, such as MKK4 in the cytosol, finally resulting in JNK phosphorylation (Nakagawa et al., 2008; Sharma et al., 2012). Consequently, pJNK translocates to the mitochondria and exacerbates oxidative stress (Hanawa et al., 2008). Finally, the mitochondrial permeability transition is induced, and apoptosis-inducing factor and endonuclease G translocates from the mitochondria to the nucleus, resulting in DNA fragmentation.

PFD, an orally bioavailable pyridine derivative, is a drug clinically used for idiopathic pulmonary fibrosis (Rosenbloom et al., 2013). PFD's antifibrotic and anti-inflammatory effects have been demonstrated in the mouse fibrosis models of the lung (Iyer et al., 1999; Iyer et al., 1995; Lehtonen et al., 2016; Oku et al., 2008; Yu et al., 2017) and in other organs (Komiya et al., 2017; Shimizu et al., 1998; Tada et al., 2001). In addition, PFD, having an antioxidative effect, has been reported to be effective for the L-arginine-induced acute pancreatitis (El-Kashef et al., 2019) and concanavalin A-induced acute liver injury models (El-Agamy, 2016). However, the precise molecular mechanism of PFD's effect is not

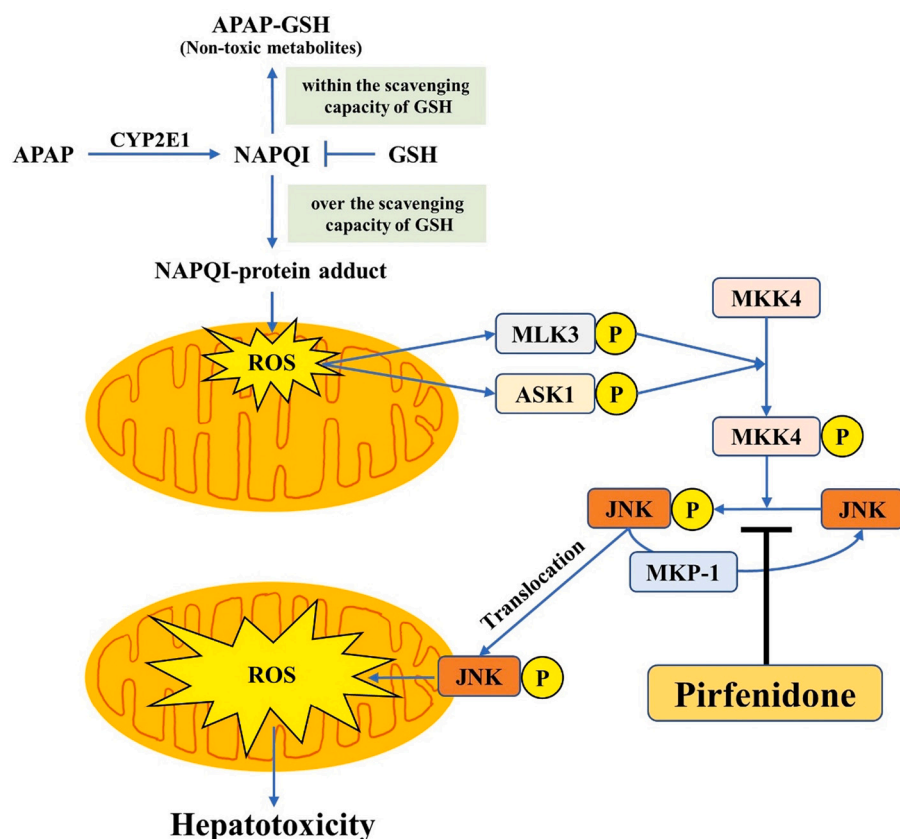


Fig. 9. APAP-induced liver injury mechanism and a supposed PFD action site.

APAP overdose causes massive NAPQI production, overwhelming GSH scavenging capacity, hence triggering mitochondrial oxidative stress. The oxidative stress activates MAPKKK, such as MLK3 and ASK1, and subsequently MAPKK, such as MKK4 in the cytosol, finally resulting in JNK phosphorylation. pJNK translocates to the mitochondria and exacerbates oxidative stress, leading to severe liver injury. Our findings indicated that PFD attenuated APAP-induced liver injury by suppressing JNK phosphorylation directly.

elucidated yet. In the present study, PFD treatment suppressed JNK phosphorylation but not MKK4 activation in vivo (Fig. 5A, B, 6A, and B). We also performed an in vitro experiment using primary hepatocytes and found comparable results: PFD suppressed JNK phosphorylation and had no effect on MKK4 activation (Fig. 7). Phosphorylated MKK4 translocates to mitochondria together with pJNK (Xie et al., 2014). While the activation of MKK4 in liver tissue was not inhibited by PFD (Fig. 6A), the translocation of pMKK4 to mitochondria was suppressed by PFD treatment (Fig. 6C). Moreover, immunoprecipitation assay showed that PFD had no effect on the binding of MKK4 to JNK (Fig. S2). PFD might suppress the translocation of pJNK into mitochondria, which result in the reduced mitochondrial translocation of pMKK4 bound to pJNK. PFD inhibits JNK activation without affecting the MKK4 activation and MKK4 binding to JNK.

MKP-1 belongs to a family of dual-specificity phosphatases and preferentially inactivates JNK-promoted stress (Hammer et al., 2006). MKP-1 deficiency enhances APAP-induced liver damage by prolonging hepatic JNK activation (Wancket et al., 2012). Moreover, Kamata et al. demonstrated that ROS induces sustained JNK activation and cell death by suppressing MKP-1 (Kamata et al., 2005). These reports suggest that MKP-1 is one of the hepatoprotective factors in APAP liver injury. In the present study, PFD did not affect MKP-1 protein expression (Fig. 6D).

Sab (also known as Sh3bp5 (SH3 domain-binding protein 5)) is a mitochondrial protein that was first identified by the yeast two-hybrid system as a binding target of phosphorylated JNK (Wiltshire et al., 2002). Win S et al. demonstrated silencing Sab interrupted the translocation of phosphorylated JNK to mitochondria, sustained activation of MKK4, and generation of mitochondrial ROS (Win et al., 2011). This suggests that pJNK-mitoSab-ROS-MKK4 activation loop plays a critical role in sustaining JNK activation. In the present study, PFD did not inhibit either ROS generation (Fig. 5D) or MKK4 activation (Fig. 6A) in the liver. Although PFD suppressed JNK phosphorylation at 3 h after APAP administration, a small amount of pJNK protein expression was

observed (Fig. 5A). We presumed that the incomplete suppression of JNK phosphorylation by PFD (Fig. 5A) might partially block the activation loop of JNK. Thus, ROS production and consequent MKK4 activation could not be suppressed by PFD (Fig. 5D and 6A). These findings suggested that PFD did not have a directive antioxidative effect in APAP-induced liver injury. Meanwhile hypercoagulation- and hypoxia-associated gene expression levels were suppressed (Fig. 3). Nuclear factor erythroid 2-related factor 2 (Nrf-2) is a transcriptional factor in the cytoplasm and leads Nrf-2 responsive genes expression such as HO-1 and HIF1 α by oxidative stress. Reduction of hypercoagulation and hypoxia by PFD may lead the suppression of oxidative stress and ROS generation. It is possible that the reduced expression of these genes reflects the inhibition of Nrf-2 pathway by PFD.

To investigate whether the inhibitory effect of PFD on JNK activation is universal, we examined the effect of PFD on JNK activation against the other model of hepatotoxicity. *Tumor Necrosis Factor α* (TNF α)/Actinomycin D (ActD) has been used as an experimental model to induce apoptosis in hepatocytes by activating caspases via JNK activation. PFD did not inhibit the phosphorylation of JNK in TNF α /ActD-induced cell death (Fig. S3). The finding indicated that the inhibitory effect of PFD on JNK activation may be specific to APAP-induced liver injury. Cell death in the LPS/GalN model is also caused by TNF α -induced apoptosis involving the TNF α receptor 1 (Leist et al., 1995) and caspase activation via JNK activation (Jaeschke et al., 1998; Küntle et al., 1997). LPS/GalN hepatotoxicity was not suppressed by PFD treatment (Fig. S4). LPS induces transcriptional activation of TNF α resulting in the induction of pro-inflammatory and anti-apoptotic genes. High dose of GalN depletes the cellular uridine triphosphate and inhibits mRNA synthesis, such as of anti-apoptotic genes, in hepatocytes, which cause the activation of the caspase cascade and DNA fragmentation. LPS/GalN hepatotoxicity eventually leads to apoptosis through activation of caspases, while APAP hepatotoxicity causes necrosis triggered by mitochondrial dysfunction without activation of caspases. Although JNK activation is involved in

various types of cell death, the stimulating factor of JNK, the downstream pathway after JNK activation, the surrounding cellular and molecular environment, and the eventual mode of cell death are quite different in each model. Suppressed JNK activation by PFD might not inhibit every type of cell death. PFD is not pan-JNK inhibitor and has a specific inhibitory effect on APAP-induced cell death. Further studies are needed to elucidate the precise mechanism for the different effects of PFD on various cell death.

Since 1969, APAP-induced liver injury is known to present liver congestion (Rose, 1969) induced by sinusoidal endothelial cell (SEC) injury and subsequent penetration of red blood cells into the Disse space (Ito et al., 2003; Ito et al., 2004; Lim et al., 1995; Walker et al., 1980, 1983, 1985). Wang et al., using photoacoustic imaging and contrast-enhanced ultrasonography on mice with APAP-induced liver injury, recently discussed that liver congestion leads to microcirculatory disturbance and parenchymal hypoxia (Wang et al., 2020). APAP is supposed to cause SEC injury both directly and indirectly via injured hepatocytes (DeLeve et al., 1997). In our study, PFD treatment significantly suppressed APAP-induced ALT elevation (Fig. 1), ameliorated TUNEL-positive hepatocyte necrosis in zone 3, inhibited oncotic necrosis due to liver congestion (Fig. 2B), and suppressed hypercoagulation- and hypoxia-associated gene expression levels (Fig. 3). Since SEC injury might be partly due to APAP-induced hepatocyte injury in zone 3, PFD could ameliorate SEC injury by suppressing hepatocyte injury and inhibiting liver congestion and subsequent hypoxic oncotic necrosis. Further studies examining the interactions between hepatocytes and SECs in APAP-induced liver injury are needed.

APAP-associated overdose is a serious problem in public health and medical economics. It accounted for about 56,000 emergency department visits and 26,000 hospitalizations and caused 458 deaths annually in the United States (Nourjah et al., 2006). NAC is the only drug approved for APAP-induced liver injury treatment so far. As we demonstrated in this study, PFD suppressed APAP-induced liver injury in a mouse model and is a promising new option to prevent APAP hepatotoxicity. Since PFD is already prescribed to idiopathic pulmonary fibrosis patients, the drug repositioning strategy could cut the cost and shorten the timeline of its clinical trial for APAP-induced liver injury. 4-Methylpyrazole (4MP) has been recommended as first-line antidote for methanol and ethylene glycol poisoning. It has been used as a therapeutic drug for a long time without any serious side effects, and its safety has been established (Rasamison et al., 2020). A previous study showed that cotreatment of 4MP with an APAP overdose effectively eliminated hepatotoxicity by inhibiting the CYP-dependent metabolic activation of APAP in mice and in human hepatocytes (Akakpo et al., 2018). It was reported that delayed administration also significantly suppressed APAP hepatotoxicity, and it is expected to be applied clinically against APAP-induced liver injury. In a murine APAP liver injury model, the inhibitory effect of 4MP on hepatotoxicity was lost when the treatment was pushed back to 3 h. Unlike 4MP, PFD was able to suppress APAP-induced liver injury even when administered 4 h after APAP administration (Fig. 8). Considering that the peak of hepatotoxicity after APAP overdose is delayed in humans (48–72 h) (Larson, 2007; McGill et al., 2012) compared to mice (12–24 h) (McGill et al., 2013), PFD can be used relatively long after APAP overdose. Although PFD is approved for idiopathic pulmonary fibrosis treatment, hepatotoxicity is one of the severe adverse events caused by PFD and liver damage exacerbated by PFD administration should be taken care in clinical practice.

5. Conclusions

Simultaneous TUNEL and vital PI staining on APAP-induced liver injury revealed that APAP-induced and typical oncotic necroses are TUNEL-positive/PI-negative and TUNEL-negative/PI-positive, respectively. PFD treatment attenuated both APAP-induced necrosis and subsequent hemorrhagic necrosis. This hepatoprotective effect against APAP-induced liver injury was exerted by suppressing JNK

phosphorylation. PFD is a promising new option to prevent APAP-induced liver injury.

Author contributions

S. Tashiro, M. Tanaka, T. Goya, M. Kohjima, M. Kato, and Y. Ogawa designed the study. S. Tashiro, M. Tanaka, T. Goya, T. Aoyagi, M. Kurakawa, K. Imoto, A. Kuwano, M. Takahashi, H. Suzuki collected data and assisted data analyses. S. Tashiro, M. Tanaka, T. Goya, M. Kohjima, M. Kato, and Y. Ogawa contributed to analysis and interpretation of data. M. Kohjima, T. Goya, M. Tanaka, M. Kato and Y. Ogawa assisted in the preparation of the manuscript and critically reviewed the manuscript. All authors approved the final version of the manuscript and agreed to be accountable for all aspects of the work in ensuring that questions related to the accuracy or integrity of any part of the work.

Declaration of competing interest

All authors have read and agree with this paper. PFD was provided by Shionogi & Co., Ltd. (Osaka, Japan).

Acknowledgment

This work was supported in part by Takeda Science Foundation [grant number TKDS20190416055], Smoking Research Foundation [grant numbers 2018G015 and 2021Y010] and JSPS KAKENHI [grant numbers JP17K09430, JP18H05039, JP19H01054, JP19K17496, JP20K22877, and JP20H04949]. We would like to thank Enago (www.enago.jp) for the English language review.

Appendix A. Supplementary data

Supplementary data to this article can be found online at <https://doi.org/10.1016/j.taap.2021.115817>.

References

- Adams, M.L., Pierce, R.H., Vail, M.E., White, C.C., Tonge, R.P., Kavanagh, T.J., Fausto, N., Nelson, S.D., Bruschi, S.A., 2001. Enhanced acetaminophen hepatotoxicity in transgenic mice overexpressing BCL-2. *Mol. Pharmacol.* 60, 907–915. <https://doi.org/10.1124/mol.60.5.907>.
- Akakpo, J.Y., Ramachandran, A., Kandel, S.E., Ni, H.M., Kumer, S.C., Rumack, B.H., Jaeschke, H., 2018. 4-Methylpyrazole protects against acetaminophen hepatotoxicity in mice and in primary human hepatocytes. *Hum. Exp. Toxicol.* 37, 1310–1322. <https://doi.org/10.1177/0960327118774902>.
- Antoine, D.J., Jenkins, R.E., Dear, J.W., Williams, D.P., McGill, M.R., Sharpe, M.R., Craig, D.G., Simpson, K.J., Jaeschke, H., Park, B.K., 2012. RETRACTED: molecular forms of HMGB1 and keratin-18 as mechanistic biomarkers for mode of cell death and prognosis during clinical acetaminophen hepatotoxicity. *J. Hepatol.* 56, 1070–1079. <https://doi.org/10.1016/j.jhep.2011.12.019>.
- Bernal, W., Auzinger, G., Dhawan, A., Wendon, J., 2010. Acute liver failure. *Lancet* 376, 190–201. [https://doi.org/10.1016/s0140-6736\(10\)60274-7](https://doi.org/10.1016/s0140-6736(10)60274-7).
- Dara, L., Johnson, H., Suda, J., Win, S., Gaarde, W., Han, D., Kaplowitz, N., 2015. Receptor interacting protein kinase 1 mediates murine acetaminophen toxicity independent of the necrosome and not through necroptosis. *Hepatology* 62, 1847–1857. <https://doi.org/10.1002/hep.27939>.
- DeLeve, L.D., Wang, X., Kaplowitz, N., Shulman, H.M., Bart, J.A., van der Hoek, A., 1997. Sinusoidal endothelial cells as a target for acetaminophen toxicity. Direct action versus requirement for hepatocyte activation in different mouse strains. *Biochem. Pharmacol.* 53, 1339–1345. [https://doi.org/10.1016/s0006-2952\(97\)00048-8](https://doi.org/10.1016/s0006-2952(97)00048-8).
- El-Agamy, D.S., 2016. Pirfenidone ameliorates concanavalin A-induced hepatitis in mice via modulation of reactive oxygen species/nuclear factor kappa B signalling pathways. *J. Pharm. Pharmacol.* 68, 1559–1566. <https://doi.org/10.1111/jphp.12651>.
- El-Kashef, D.H., Shaaban, A.A., El-Agamy, D.S., 2019. Protective role of pirfenidone against experimentally-induced pancreatitis. *Pharmacol. Rep.* 71, 774–781. <https://doi.org/10.1016/j.pharep.2019.04.005>.
- Ferret, P.J., Hammoud, R., Tulliez, M., Tran, A., Trébédien, H., Jaffray, P., Malassagne, B., Calmus, Y., Weill, B., Batteux, F., 2001. Detoxification of reactive oxygen species by a nonpeptidyl mimic of superoxide dismutase cures acetaminophen-induced acute liver failure in the mouse. *Hepatology* 33, 1173–1180. <https://doi.org/10.1053/jhep.2001.24267>.
- Fisher, E.S., Curry, S.C., 2019. Evaluation and treatment of acetaminophen toxicity. *Adv. Pharmacol.* 85, 263–272. <https://doi.org/10.1016/bs.apha.2018.12.004>.

- Gujral, J.S., Knight, T.R., Farhood, A., Bajt, M.L., Jaeschke, H., 2002. Mode of cell death after acetaminophen overdose in mice: apoptosis or oncotic necrosis? *Toxicol. Sci.* 67, 322–328. <https://doi.org/10.1093/toxsci/67.2.322>.
- Hammer, M., Mages, J., Dietrich, H., Servatius, A., Howells, N., Cato, A.C., Lang, R., 2006. Dual specificity phosphatase 1 (DUSP1) regulates a subset of LPS-induced genes and protects mice from lethal endotoxin shock. *J. Exp. Med.* 203, 15–20. <https://doi.org/10.1084/jem.20051753>.
- Hanawa, N., Shinohara, M., Saberi, B., Gaarde, W.A., Han, D., Kaplowitz, N., 2008. Role of JNK translocation to mitochondria leading to inhibition of mitochondria bioenergetics in acetaminophen-induced liver injury. *J. Biol. Chem.* 283, 13565–13577. <https://doi.org/10.1074/jbc.M708916200>.
- Hu, J., Lemasters, J.J., 2020. Suppression of iron mobilization from lysosomes to mitochondria attenuates liver injury after acetaminophen overdose in vivo in mice: protection by minocycline. *Toxicol. Appl. Pharmacol.* 392, 114930 <https://doi.org/10.1016/j.taap.2020.114930>.
- Imagawa, Y., Saitoh, T., Tsujimoto, Y., 2016. Vital staining for cell death identifies Atg9a-dependent necrosis in developmental bone formation in mouse. *Nat. Commun.* 7, 13391. <https://doi.org/10.1038/ncomms13391>.
- Ito, Y., Bethea, N.W., Abril, E.R., McCuskey, R.S., 2003. Early hepatic microvascular injury in response to acetaminophen toxicity. *Microcirculation* 10, 391–400. <https://doi.org/10.1038/sj.mn.7800204>.
- Ito, Y., Machen, N.W., Abril, E.R., McCuskey, R.S., 2004. Effects of acetaminophen on hepatic microcirculation in mice. *Comp. Hepatol.* 3 (Suppl. 1), S33. <https://doi.org/10.1186/1476-5926-2-s1-s33>.
- Iyer, S.N., Wild, J.S., Schiedt, M.J., Hyde, D.M., Margolin, S.B., Giri, S.N., 1995. Dietary intake of pirfenidone ameliorates bleomycin-induced lung fibrosis in hamsters. *J. Lab. Clin. Med.* 125, 779–785.
- Iyer, S.N., Gurujeyalakshmi, G., Giri, S.N., 1999. Effects of pirfenidone on transforming growth factor-beta gene expression at the transcriptional level in bleomycin hamster model of lung fibrosis. *J. Pharmacol. Exp. Ther.* 291, 367–373.
- Jaeschke, H., Fisher, M.A., Lawson, J.A., Simmons, C.A., Farhood, A., Jones, D.A., 1998. Activation of caspase 3 (CPP32)-like proteases is essential for TNF-alpha-induced hepatic parenchymal cell apoptosis and neutrophil-mediated necrosis in a murine endotoxin shock model. *J. Immunol.* 160, 3480–3486.
- Jaeschke, H., Cover, C., Bajt, M.L., 2006. Role of caspases in acetaminophen-induced liver injury. *Life Sci.* 78, 1670–1676. <https://doi.org/10.1016/j.lfs.2005.07.003>.
- Jaeschke, H., Duan, L., Akakpo, J.Y., Farhood, A., Ramachandran, A., 2018. The role of apoptosis in acetaminophen hepatotoxicity. *Food Chem. Toxicol.* 118, 709–718. <https://doi.org/10.1016/j.fct.2018.06.025>.
- Jaeschke, H., Ramachandran, A., Chao, X., Ding, W.X., 2019. Emerging and established modes of cell death during acetaminophen-induced liver injury. *Arch. Toxicol.* 93, 3491–3502. <https://doi.org/10.1007/s00204-019-02597-1>.
- Julien, O., Wells, J.A., 2017. Caspases and their substrates. *Cell Death Differ.* 24, 1380–1389. <https://doi.org/10.1038/cdd.2017.44>.
- Kamata, H., Honda, S., Maeda, S., Chang, L., Hirata, H., Karin, M., 2005. Reactive oxygen species promote TNFalpha-induced death and sustained JNK activation by inhibiting MAP kinase phosphatases. *Cell* 120, 649–661. <https://doi.org/10.1016/j.cell.2004.12.041>.
- Kanno, S., Ishikawa, M., Takayanagi, M., Takayanagi, Y., Sasaki, K., 2000. Potentiation of acetaminophen hepatotoxicity by doxapram in mouse primary cultured hepatocytes. *Biol. Pharm. Bull.* 23, 446–450. <https://doi.org/10.1248/bpb.23.446>.
- Komiyama, C., Tanaka, M., Tsuchiya, K., Shimazu, N., Mori, K., Furuke, S., Miyachi, Y., Shiba, K., Yamaguchi, S., Ikeda, K., Ochi, K., Nakabayashi, K., Hata, K.I., Itoh, M., Suganami, T., Ogawa, Y., 2017. Antifibrotic effect of pirfenidone in a mouse model of human nonalcoholic steatohepatitis. *Sci. Rep.* 7, 44754. <https://doi.org/10.1038/srep44754>.
- Künstle, G., Leist, M., Uhlig, S., Revesz, L., Feifel, R., MacKenzie, A., Wendel, A., 1997. ICE-protease inhibitors block murine liver injury and apoptosis caused by CD95 or by TNF-alpha. *Immunol. Lett.* 55, 5–10. [https://doi.org/10.1016/s0165-2478\(96\)02642-9](https://doi.org/10.1016/s0165-2478(96)02642-9).
- Larson, A.M., 2007. Acetaminophen hepatotoxicity. *Clin. Liver Dis.* 11 (525–548), vi. <https://doi.org/10.1016/j.cld.2007.06.006>.
- Lawson, J.A., Fisher, M.A., Simmons, C.A., Farhood, A., Jaeschke, H., 1999. Inhibition of Fas receptor (CD95)-induced hepatic caspase activation and apoptosis by acetaminophen in mice. *Toxicol. Appl. Pharmacol.* 156, 179–186. <https://doi.org/10.1006/taap.1999.8635>.
- Lee, W.M., 2012. Acute liver failure. *Semin. Respir. Crit. Care Med.* 33, 36–45. <https://doi.org/10.1055/s-0032-1301733>.
- Lee, W.M., 2017. Acetaminophen (APAP) hepatotoxicity-Isn't it time for APAP to go away? *J. Hepatol.* 67, 1324–1331. <https://doi.org/10.1016/j.jhep.2017.07.005>.
- Lehtonen, S.T., Veijola, A., Karvonen, H., Lappi-Blanco, E., Sormunen, R., Korpela, S., Zagai, U., Sköld, M.C., Kaarteenaho, R., 2016. Pirfenidone and nintedanib modulate properties of fibroblasts and myofibroblasts in idiopathic pulmonary fibrosis. *Respir. Res.* 17, 14. <https://doi.org/10.1186/s12931-016-0328-5>.
- Leist, M., Gantner, F., Jilg, S., Wendel, A., 1995. Activation of the 55 kDa TNF receptor is necessary and sufficient for TNF-induced liver failure, hepatocyte apoptosis, and nitrite release. *J. Immunol.* 154, 1307–1316.
- Lim, S.P., Andrews, F.J., O'Brien, P.E., 1995. Acetaminophen-induced microvascular injury in the rat liver: protection with misoprostol. *Hepatology* 22, 1776–1781.
- Maeda, S., Chang, L., Li, Z.W., Luo, J.L., Leftert, H., Karin, M., 2003. IKKbeta is required for prevention of apoptosis mediated by cell-bound but not by circulating TNFalpha. *Immunity* 19, 725–737. [https://doi.org/10.1016/s1074-7613\(03\)00301-7](https://doi.org/10.1016/s1074-7613(03)00301-7).
- McGill, M.R., Jaeschke, H., 2013. Metabolism and disposition of acetaminophen: recent advances in relation to hepatotoxicity and diagnosis. *Pharm. Res.* 30, 2174–2187. <https://doi.org/10.1007/s11095-013-1007-6>.
- McGill, M.R., Sharpe, M.R., Williams, C.D., Taha, M., Curry, S.C., Jaeschke, H., 2012. The mechanism underlying acetaminophen-induced hepatotoxicity in humans and mice involves mitochondrial damage and nuclear DNA fragmentation. *J. Clin. Invest.* 122, 1574–1583. <https://doi.org/10.1172/jci59755>.
- McGill, M.R., Lebofsky, M., Norris, H.R., Slawson, M.H., Bajt, M.L., Xie, Y., Williams, C.D., Wilkins, D.G., Rollins, D.E., Jaeschke, H., 2013. Plasma and liver acetaminophen-protein adduct levels in mice after acetaminophen treatment: dose-response, mechanisms, and clinical implications. *Toxicol. Appl. Pharmacol.* 269, 240–249. <https://doi.org/10.1016/j.taap.2013.03.026>.
- Nakagawa, H., Maeda, S., Hikiba, Y., Ohmae, T., Shibata, W., Yanai, A., Sakamoto, K., Ogura, K., Noguchi, T., Karin, M., Ichijo, H., Omata, M., 2008. Deletion of apoptosis signal-regulating kinase 1 attenuates acetaminophen-induced liver injury by inhibiting c-Jun N-terminal kinase activation. *Gastroenterology* 135, 1311–1321. <https://doi.org/10.1053/j.gastro.2008.07.006>.
- Niknahad, H., Heidari, R., Mohammadzadeh, R., Ommati, M.M., Khodaei, F., Azarpina, N., Abdoli, N., Zarei, M., Asadi, B., Rasti, M., Shirazi Yeganeh, B., Taheri, V., Saeedi, A., Najibi, A., 2017. Sulfasalazine induces mitochondrial dysfunction and renal injury. *Ren. Fail.* 39, 745–753. <https://doi.org/10.1080/0886022x.2017.1399908>.
- Nourjah, P., Ahmad, S.R., Karwoski, C., Willy, M., 2006. Estimates of acetaminophen (Paracetamol)-associated overdoses in the United States. *Pharmacoepidemiol. Drug Saf.* 15, 398–405. <https://doi.org/10.1002/pds.1191>.
- Oku, H., Shimizu, T., Kawabata, T., Nagira, M., Hikita, I., Ueyama, A., Matsushima, S., Torii, M., Arimura, A., 2008. Antifibrotic action of pirfenidone and prednisolone: different effects on pulmonary cytokines and growth factors in bleomycin-induced murine pulmonary fibrosis. *Eur. J. Pharmacol.* 590, 400–408. <https://doi.org/10.1016/j.ejphar.2008.06.046>.
- Ramachandran, A., McGill, M.R., Xie, Y., Ni, H.M., Ding, W.X., Jaeschke, H., 2013. Receptor interacting protein kinase 3 is a critical early mediator of acetaminophen-induced hepatocyte necrosis in mice. *Hepatology* 58, 2099–2108. <https://doi.org/10.1002/hep.26547>.
- Rasamison, R., Besson, H., Berleux, M.P., Schicchi, A., Mégarbane, B., 2020. Analysis of fomepizole safety based on a 16-year post-marketing experience in France. *Clin. Toxicol. (Phila.)* 58, 742–747. <https://doi.org/10.1080/15563650.2019.1676899>.
- Ray, S.D., Mumaw, V.R., Raje, R.R., Fariss, M.W., 1996. Protection of acetaminophen-induced hepatocellular apoptosis and necrosis by cholesteryl hemisuccinate pretreatment. *J. Pharmacol. Exp. Ther.* 279, 1470–1483.
- Rose, P.G., 1969. Paracetamol overdose and liver damage. *Br. Med. J.* 1, 381–382. <https://doi.org/10.1136/bmj.1.5640.381-a>.
- Rosenbloom, J., Mendoza, F.A., Jimenez, S.A., 2013. Strategies for anti-fibrotic therapies. *Biochim. Biophys. Acta* 1832, 1088–1103. <https://doi.org/10.1016/j.bbdis.2012.12.007>.
- Sharma, M., Gadang, V., Jaeschke, A., 2012. Critical role for mixed-lineage kinase 3 in acetaminophen-induced hepatotoxicity. *Mol. Pharmacol.* 82, 1001–1007. <https://doi.org/10.1124/mol.112.079863>.
- Shimizu, T., Kuroda, T., Hata, S., Fukagawa, M., Margolin, S.B., Kurokawa, K., 1998. Pirfenidone improves renal function and fibrosis in the post-obstructed kidney. *Kidney Int.* 54, 99–109. <https://doi.org/10.1046/j.1523-1755.1998.00962.x>.
- Tada, S., Nakamura, M., Enjoji, M., Sugimoto, R., Iwamoto, H., Kato, M., Nakashima, Y., Nawata, H., 2001. Pirfenidone inhibits dimethylnitrosamine-induced hepatic fibrosis in rats. *Clin. Exp. Pharmacol. Physiol.* 28, 522–527. <https://doi.org/10.1046/j.1440-1681.2001.03481.x>.
- Thomas, S.H., 1993. Paracetamol (acetaminophen) poisoning. *Pharmacol. Ther.* 60, 91–120. [https://doi.org/10.1016/0163-7258\(93\)90023-7](https://doi.org/10.1016/0163-7258(93)90023-7).
- Thornberry, N.A., 1997. The caspase family of cysteine proteases. *Br. Med. Bull.* 53, 478–490. <https://doi.org/10.1093/oxfordjournals.bmb.a011625>.
- Tsurusaki, S., Tsuchiya, Y., Koumura, T., Nakasone, M., Sakamoto, T., Matsuoka, M., Imai, H., Yuet-Yin Kok, C., Okochi, H., Nakano, H., Miyajima, A., Tanaka, M., 2019. Hepatic ferroptosis plays an important role as the trigger for initiating inflammation in nonalcoholic steatohepatitis. *Cell Death Dis.* 10, 449. <https://doi.org/10.1038/s41419-019-1678-y>.
- Walker, R.M., Racz, W.J., McElligott, T.F., 1980. Acetaminophen-induced hepatotoxicity in mice. *Lab. Invest.* 42, 181–189.
- Walker, R.M., Racz, W.J., McElligott, T.F., 1983. Scanning electron microscopic examination of acetaminophen-induced hepatotoxicity and congestion in mice. *Am. J. Pathol.* 113, 321–330.
- Walker, R.M., Racz, W.J., McElligott, T.F., 1985. Acetaminophen-induced hepatotoxic congestion in mice. *Hepatology* 5, 233–240. <https://doi.org/10.1002/hep.1840050213>.
- Wancket, L.M., Meng, X., Rogers, L.K., Liu, Y., 2012. Mitogen-activated protein kinase phosphatase (Mkp)-1 protects mice against acetaminophen-induced hepatic injury. *Toxicol. Pathol.* 40, 1095–1105. <https://doi.org/10.1177/0192623312447551>.
- Wang, H., Burke, L.J., Patel, J., Tse, B.W., Bridle, K.R., Cogger, V.C., Li, X., Liu, X., Yang, H., Crawford, D.H.G., Roberts, M.S., Gao, W., Liang, X., 2020. Imaging-based vascular-related biomarkers for early detection of acetaminophen-induced liver injury. *Theranostics* 10, 6715–6727. <https://doi.org/10.7150/thno.44900>.
- Wiltshire, C., Matsushita, M., Tsukada, S., Gillespie, D.A., May, G.H., 2002. A new c-Jun N-terminal kinase (JNK)-interacting protein, sab (SH3BP5), associates with mitochondria. *Biochem. J.* 367, 577–585. <https://doi.org/10.1042/bj20020553>.
- Wimborne, H.J., Hu, J., Takemoto, K., Nguyen, N.T., Jaeschke, H., Lemasters, J.J., Zhong, Z., 2020. Aldehyde dehydrogenase-2 activation decreases acetaminophen hepatotoxicity by prevention of mitochondrial depolarization. *Toxicol. Appl. Pharmacol.* 396, 114982. <https://doi.org/10.1016/j.taap.2020.114982>.
- Win, S., Than, T.A., Han, D., Petrovic, L.M., Kaplowitz, N., 2011. C-Jun N-terminal kinase (JNK)-dependent acute liver injury from acetaminophen or tumor necrosis factor

- (TNF) requires mitochondrial sab protein expression in mice. *J. Biol. Chem.* 286, 35071–35078. <https://doi.org/10.1074/jbc.M111.276089>.
- Xie, Y., McGill, M.R., Dorko, K., Kumer, S.C., Schmitt, T.M., Forster, J., Jaeschke, H., 2014. Mechanisms of acetaminophen-induced cell death in primary human hepatocytes. *Toxicol. Appl. Pharmacol.* 279, 266–274. <https://doi.org/10.1016/j.taap.2014.05.010>.
- Yamada, N., Karasawa, T., Kimura, H., Watanabe, S., Komada, T., Kamata, R., Sampilvanjil, A., Ito, J., Nakagawa, K., Kuwata, H., Hara, S., Mizuta, K., Sakuma, Y., Sata, N., Takahashi, M., 2020. Ferroptosis driven by radical oxidation of n-6 polyunsaturated fatty acids mediates acetaminophen-induced acute liver failure. *Cell Death Dis.* 11, 144. <https://doi.org/10.1038/s41419-020-2334-2>.
- Yu, W., Guo, F., Song, X., 2017. Effects and mechanisms of pirfenidone, prednisone and acetylcysteine on pulmonary fibrosis in rat idiopathic pulmonary fibrosis models. *Pharm. Biol.* 55, 450–455. <https://doi.org/10.1080/13880209.2016.1247879>.
- Zhang, H., Cook, J., Nickel, J., Yu, R., Stecker, K., Myers, K., Dean, N.M., 2000. Reduction of liver Fas expression by an antisense oligonucleotide protects mice from fulminant hepatitis. *Nat. Biotechnol.* 18, 862–867. <https://doi.org/10.1038/78475>.
- Zhang, Y.F., He, W., Zhang, C., Liu, X.J., Lu, Y., Wang, H., Zhang, Z.H., Chen, X., Xu, D. X., 2014. Role of receptor interacting protein (RIP)1 on apoptosis-inducing factor-mediated necroptosis during acetaminophen-evoked acute liver failure in mice. *Toxicol. Lett.* 225, 445–453. <https://doi.org/10.1016/j.toxlet.2014.01.005>.
- Zhang, J., Min, R.W.M., Le, K., Zhou, S., Aghajan, M., Than, T.A., Win, S., Kaplowitz, N., 2017. The role of MAP2 kinases and p38 kinase in acute murine liver injury models. *Cell Death Dis.* 8, e2903 <https://doi.org/10.1038/cddis.2017.295>.